Analyzing time-resolved spectroscopic data from an azimuthally symmetric, aluminum-wire array, *z*-pinch implosion

K. G. Whitney, J. W. Thornhill, P. E. Pulsifer, and J. P. Apruzese
Radiation Hydrodynamics Branch, Plasma Physics Division, Naval Research Laboratory, Washington, D.C. 20375

T. W. L. Sanford, T. J. Nash, R. C. Mock, and R. B. Spielman
Sandia National Laboratories P.O. Box 5800, Albuquerque, New Mexico 87185
(Received 10 December 1996; revised manuscript received 13 February 1997)

A 90-wire, aluminum, *z*-pinch experiment was conducted on the Saturn accelerator at the Sandia National Laboratories that exhibited azimuthally symmetric implosions and two x-ray bursts, a main burst and a subsidiary one. These bursts correlated with two consecutive radial implosions and are consistent with predicted magnetohydrodynamics behavior. A variety of time-resolved, accurately timed, spectroscopic measurements were made in this experiment and are described in this paper. These measurements include (1) the pinch implosion time, (2) time-resolved pinhole pictures that give sizes of the *K*-shell emission region, (3) time-resolved *K*-series spectra that give the relative amounts of hydrogenlike to heliumlike to continuum emission, (4) the total and the *K*-shell x-ray power outputs, and (5) time-resolved photoconducting diode measurements from which continuum slopes and time-resolved electron temperatures can be inferred. Time-resolved Ly-α and Ly-β linewidths are obtained from the spectra and inferences about time-resolved ion temperatures are also made. All of these data correlate well with one another. A method is then presented of analyzing this data that relies on the complete set of time-resolved measurements. This analysis utilizes one-dimensional radiative magnetohydrodynamic simulations of the experiments, which drive *z*-pinch implosions using the measured Saturn circuit parameters. These simulations are used to calculate the same x-ray quantities as were measured. Then, comparisons of the measured and calculated data are shown to define a process by which different dynamical assumptions can be invoked or rejected in an attempt to reproduce the ensemble of data. This process depends on the full data set and provides insight into the structure of the radial temperature and density gradients of the on-axis pinch. It implies that the first implosion is composed of a hot plasma core, from which the kilovolt emissions emanate, surrounded by a cooler, denser shell, and it provides details about the structure of the temperature and density gradients between the core and shell regions. These results are found to be broadly consistent with an earlier, less detailed, data analysis in which plasma gradients are ignored. However, the ability to reproduce the full spectroscopic data in the present analysis is found to be sensitively dependent on the radial gradients that are calculated. [S1063-651X(97)06609-9]

PACS number(s): 52.30.−q, 52.70.La

I. INTRODUCTION

Calculations of *z*-pinch dynamics are generally approximate in their treatment of either the geometry, the spatial resolution, or the nonlinear plasma chemistry of the fluid flow. Consequently, detailed comparisons of calculated x-ray data (such as powers, line ratios, and continuum slopes) with the same quantities extracted from experimental measurements have inherent limitations. Some limitations can be reduced by conducting experiments that more closely approximate the geometric assumptions, such as cylindrical or translational symmetry, that are most often made in the calculations. The 90-wire aluminum array experiment that is analyzed in this paper comes close to meeting this goal. The use of large wire numbers reduces the degree of azimuthal asymmetry of the imploding plasma. It also improves the shot-to-shot reproducibility of the implosion and the degree of cylindrical symmetry that is achieved by the pinch on axis as measured in *K*-shell spectrum x rays.

On the other hand, overcoming inherent limitations imposed on radiative magneto-hydrodynamic code (RMHC) calculations by the inability to adequately spatially resolve the fluid dynamics or to numerically integrate the full ionization and radiation transport dynamics is a more difficult problem. In this case, diagnostic procedures need to be developed that can be used to test the effect that the RMHC approximations have on their ability to replicate experimental results. In the work to be presented in this paper, an extensive atomic model of aluminum was used, which is described at the beginning of Sec. III, to carry out this diagnostic development. A variety of well-posed, and successively more complicated, theoretical calculations that both exclude and include the effects of hydrodynamic motions need to be developed so that they can be used to analyze experimental data. Prediction of the data from first principles is a more challenging, and essentially unrealistic, objective that is ultimately facilitated by such analyses as will be described. We will see more of what this statement means as we proceed.

A nondynamical, diagnostic perspective is illustrated by the use of detailed collisional-radiative ionization equilibrium (CRE) calculations to infer an average emission electron temperature $\langle T_e \rangle$ or ion density $\langle N_i \rangle$ from an x-ray spectrum emitted from a transient, laboratory plasma. All effects related to the coupling of the ionization dynamics to the plasma fluid flow or to the radiation field are ignored in

 © 1997 The American Physical Society

applying these calculations as a plasma diagnostic, e.g., no ladder ionization via photopumping is included in the calculations. Uniform plasma conditions are assumed in order to infer a limited set of two plasma quantities, $\langle T_e \rangle$ and $\langle N_i \rangle$, from two spectral input quantities, i.e., gradient, time history, and fluid turbulence effects are all left undiagnosed. More recently, the application of these procedures to z-pinch plasmas has been extended to include the effects of radiation-field interactions, i.e., photoexcitations and ionizations, in optically thick plasmas [1,2]. In this case, a new piece of information, the emission region size, is used as input to the calculation, and a new piece of information, the mass of the emission region, is inferred as output.

In the 90-wire pinch experiment to be analyzed in this paper, an extensive set of time-resolved x-ray measurements was made. We discuss this experiment separately [3] and it is also discussed in Refs. [4–6]. The experiment was repeated three times. These three shots had two important characteristics: one, they were highly reproducible by z-pinch standards, and two, the pinhole data they generated was suggestive of approximate, one-dimensional (1D), cylindrically symmetric, implosion behavior. The data consisted of (1) the measured implosion time, i.e., measured current traces and the K-shell x-ray pulse relative to the current trace, (2) the total x-ray power output pulse, (3) the K-shell power pulse, (4) seven time-resolved and accurately timed K-shell pinhole pictures per shot from which the size of the K-shell radiating region as a function of time as well as the implosion time were determined, (5) seven time-resolved and accurately timed K-series spectra per shot from which line ratios as a function of time, especially that of the H-like Ly-α line emission to the He-like $n=2$-1 emissions, were determined, and (6) time-resolved electron temperatures that were inferred from the slope of radiative recombination emission as measured by photoconducting diodes [7] (PCDs) or as extracted from the K-series spectra. Spatially resolved, but time-integrated, pinhole pictures were also recorded, but they are not used in the analysis of this paper. They will be described in a forthcoming paper [8].

A CRE analysis of these data, taken together with an analysis of the free-bound continuum slope, led to an early conclusion that the pinched plasma contained steep temperature gradients [4], i.e., it contained a hot core surrounded by a cooler plasma halo. A similar tentative conclusion was drawn from an analysis of emission data obtained in a mixture experiment in which magnesium was coated onto aluminum wires [9]. Clearly, these gradients have a major influence on the plasma dynamics and on the emission characteristics of the pinch, and consequently, it is vital that they be accurately diagnosed if possible. The problem is that these gradients depend, in general, on the full time history of the implosion dynamics. Consequently, the degree to which the data can presently be reproduced by a 1D RMHC calculation, and under what assumptions, is investigated in this paper as an important step towards developing a diagnostic for both gradients and the dynamics behind their development.

The nonlinearity of z-pinch dynamics makes it generally difficult to obtain complete agreement with all of the data through the adjustment of calculational assumptions. However, in the analysis of the 90-wire experiment, it was found that changes in these assumptions moved one or another of the calculated data toward either closer agreement or greater disagreement with the measured data. Therefore the process of seeking agreement leads, in principle, to an unambiguous set of physical assumptions offering the best matchup and, therefore, the best diagnostic of the data. The results to be presented in this paper illustrate some of what can be learned by this process, and a number of important, though still tentative, conclusions are drawn from it.

The comparisons that are made in this paper between calculated and experimentally measured x-ray data do not show perfect agreement between the two data sets. The best agreement is obtained between the emitted K-shell powers. This quantity, like the total x-ray power (the sum of both subkilovolt and superkilovolt emissions), is most sensitive to the degree of compressibility of the assembled plasma and to the distribution of energy within it. The comparison of the K-shell powers is in better agreement than that of the total powers because the calculated total power depends on more of the detailed structure of the atomic model used in the calculation than does the K-shell power. Line ratios, continuum slopes, and Doppler linewidths, on the other hand, are sensitive to the structure of the temperature and density gradients that are generated in the experiment and that are calculated. Detailed agreement, especially in time, is therefore more difficult to obtain between these calculated and measured quantities. It is also dependent on the ionization dynamics of the plasma, and there are approximations that generally must be made in the calculation that are not generally valid throughout the experimental plasma dynamics. Nevertheless, the comparisons between line ratios and continuum slopes that are shown in this paper are generally good, though not perfect, and they point the way toward improved understanding of the z-pinch dynamics, which, even if it cannot be replicated with perfection, can be somewhat accurately bounded.

A description of the 90-wire experiment, its symmetry, reproducibility, and the time-resolved spectroscopic data that were acquired, is presented in Sec. II. Several preliminary, non-RMHC, analyses of the experiment are then discussed in Sec. III. In Sec. IV our ability to model the pulse power energy flow and to simulate the implosion dynamics is discussed, and the process of interpreting the data using 1D simulations is described. These simulations attempt to model some 3D effects phenomenologically. Comparisons are made between the experimental data and the same set of calculated data obtained using the Naval Research Laboratory's RMHC [10,11] to simulate the experiment. These comparisons address the question of how well the gradient structure of a z pinch can be diagnosed, and the physics of z-pinch gradients probed, by the ability of a 1D RMHC to replicate time-resolved spectroscopic measurements. Preliminary conclusions on the viability of this process are drawn in Sec. V.

II. DESCRIPTION OF THE EXPERIMENT

The experiment to be analyzed was conducted with 2-cm-long arrays, 1.72 cm in diameter, composed of 90, 13-μm-diam aluminum wires having a total mass of 615 μg. Three shots were taken, labeled 2085, 2094, and 2095. Because of their high degree of reproducibility, we have treated the three

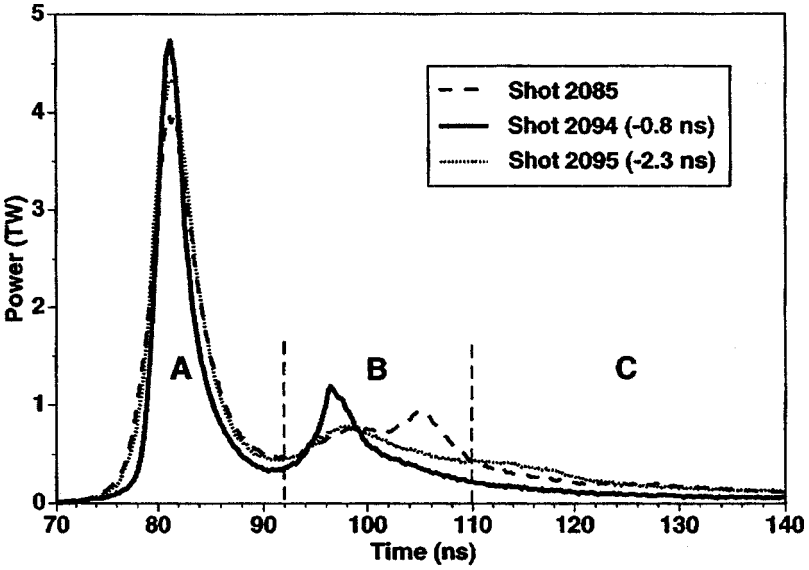

FIG. 1. *K*-shell power outputs versus time. The power pulses for the three shots are superposed by shifting shots 2094 and 2095 by the amounts indicated.

separate data sets from these shots as one and have analyzed the data as if they were from one shot. The reproducibility of the *K*-shell power pulse is illustrated in Fig. 1. The power curve from shot 2094 was shifted by -0.8 ns and the power from shot 2095 by -2.3 ns to bring the three main peaks, labeled *A*, into coincidence. Each of these peaks has approximately a 4-ns full width at half maximum (FWHM) and a peak of 4.3 ± 0.4 TW. A second, smaller peak follows the main peak. Figure 1 shows that this secondary peak is the least reproducible part of the power pulse.

A pinhole picture of the pinch at peak power is shown in Fig. 2. The x rays were filtered so that only kilovolt emissions were recorded, i.e., only the *K*-shell emissions of aluminum. A radial densitometer trace of this picture, averaged over the axial, *z*, direction shows that a tight, well-defined pinch, 0.62 mm in diameter, had formed [4,3]. Figure 2 suggests that this pinch was fairly uniform in *z*, although densitometer traces along the axial direction show that periodic structure was present both before and after peak power [3]. The small pinch radius suggests that the effects of current-driven asymmetries, array nonuniformities, and unequal $\mathbf{j} \times \mathbf{B}$ forces due to the finite number of return current posts were small in these experiments.

Because time-resolved measurements were made, the evolution of the pinch during assembly could be studied. A series of eight pinhole pictures, taken in *K*-shell x rays, was recorded for shot 2085. They are shown in Fig. 3 for a succession of times; peak compression, at 81.5 ns, occurs in the second frame. The pictures show a shell of plasma (frame 1) imploding to the axis, forming a tight pinch (frame 2), reexpanding (frames 3–7), and then recompressing (frame 8). This overall picture is consistent with the power curve shown in Fig. 1. One can use densitometer traces of the pinhole pictures, averaged over *z*, to determine the average or mean size of the *K*-shell emission region as a function of time. Figure 4 contains all of these measured sizes (the FWHM of Gaussian fits to core regions that sit atop a ~ 3.2-mm Gaussian halo) drawn relative to the power pulse from shot 2094. A curve interpolating the position of the pinch, defined by an average over the three shots, is also drawn. The error bars

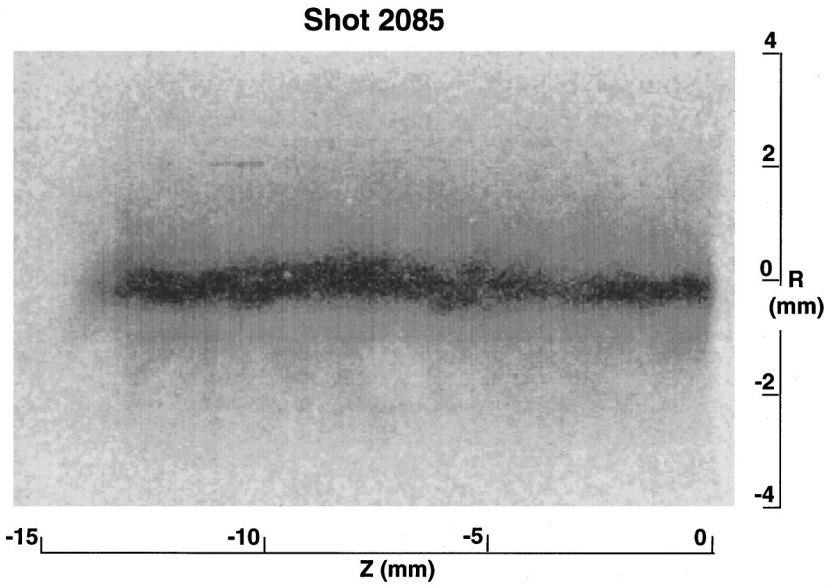

FIG. 2. Time-resolved pinhole camera (TRPHC) picture of shot 2094 taken at approximately the time of peak compression. Lineouts (i.e., densitometer traces across the film) in *r* or *z* show a tight, approximately uniform, pinch.

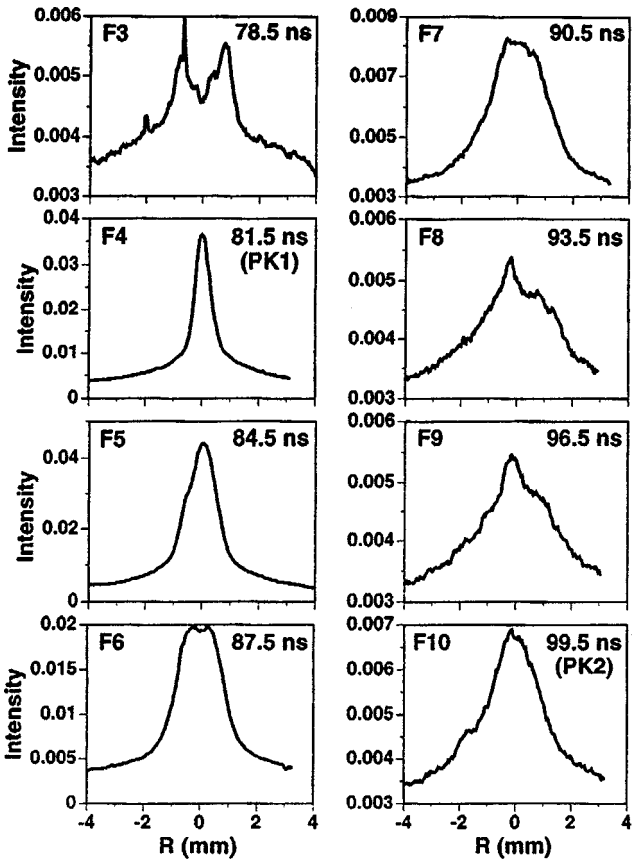

FIG. 3. Lineouts, averaged over z, as a function of time of the relative film intensity of K-shell pinhole pictures taken with the small format camera. These intensities show a plasma shell imploding to the axis, forming a tight approximately uniform pinch, reexpanding, and then recompressing.

represent timing uncertainties (see the discussion of Fig. 1) and the rms shot-to-shot variations in deriving sizes from the changing, z-dependent, radial shape of the pinch. Radial asymmetries are seen in the pinhole pictures, although they appear to be mild. This observation is consistent with current measurements that were made, which are presented in Sec. III.

Measurements of the total (unfiltered) power output from the pinch were also made (Fig. 5). Like the K-shell power, they exhibit a main peak and a smaller, secondary peak, both correlated with the K-shell peaks. The peak of the total power is approximately six times the size of the K-shell peak. Note that the timing uncertainties are slightly different for the total power than for the K-shell power pulses, i.e., slightly different shifts were needed to bring the total power pulses into coincidence than were needed for the K-shell pulses.

In addition to the pinhole pictures, a set of time-resolved K-series spectra was recorded in each of the three shots. They are presented in Fig. 6 for shots 2085, 2094, and 2095 ordered by time. From these spectra, a variety of information was obtained: ratios of hydrogenlike to heliumlike line emission as well as line profiles and linewidths. The data from the three shots, when plotted versus time, present a consistent picture of the 90-wire emission dynamics when compared with both the power pulses of Fig. 1 and the emission region sizes of Fig. 4. For example, the Ly-α to He-α (including intercombination line) ratio, for the three shots, together show that hydrogenlike emission reaches its maximum relative to heliumlike emission at ~ 5 ns following peak compression. The ratio subsequently falls, only to reach a second, smaller maximum at the time of the second power peak. The ion temperatures that are inferred from the relative Ly-α and Ly-β linewidths of the three shots also rise and fall with the power pulse (see Ref. [3]) as do the electron temperatures that are inferred from the continuum slope as measured by PCD detectors (Ref. [4]).

The reproducibility and consistency of the spectroscopic data promote their use as a single, substantial, data set with which to analyze and diagnose the 90-wire experiment. Several methods have been employed. In a companion paper (Ref. [3]), a 2D RMHC analysis is described, which is supported by the z-dependent structure observed in the pinch. Another, 1D, method of analysis is suggested by the smallness of the radial asymmetry present in the pinhole pictures and by the appearance of a bounce and pinch recompression. Both of these observations support the use of 1D RMHC simulations to investigate the dynamics of plasma assembly. However, an important guide to this investigation is provided by several non-RMHC analyses of the spectral data, described in the following section.

III. NON-RMHC ANALYSES OF THE EXPERIMENT

Two measurements, shown in Fig. 7, were made of the diode current, labeled I_{BV1} and I_{BV2} (where BV refers to a B-dot sensor mounted on a vertical with respect to the z pinch). One measurement, I_{BV2}, was positioned adjacent to one of the ten return current posts. The other was located approximately 180° from I_{BV2}; it was shifted slightly to lie midway between two return current posts. The average, I_{av}, of these currents is also drawn in Fig. 7. Because the detectors were identical, these measurements, which were reproducible, suggest that the current distribution in the load, and therefore the implosion, could be somewhat asymmetrical and nonideal. Some of the residual nonreproducibility of the three shots may be attributable to this asymmetry. Note that it will also somewhat corrupt data analyses that are based on the assumption of locally, cylindrically, symmetric implosions.

Several data analyses, not involving RMHC calculations, imply that steep gradients in temperature and density were produced when the 90-wire array assembled on axis. Each analysis involves a determination of the mass participating in one part of the pinch dynamics or another. For example, a simple (slug model) circuit analysis shows that the measured implosion time is consistent with the measured diode current and the Saturn circuit model only if the full array mass is imploded. Thus, based on implosion time and current measurements, one must account for the full array mass in one part or another of the emission dynamics on axis.

A second analysis of both time-resolved line and continuum emissions is described in Ref. [4]. The line analysis in this reference utilized line ratios taken from the time-resolved, but spatially unresolved, K-shell spectra of Fig. 6, emission region sizes taken from the average position curve in Fig. 4, and the average power data from Fig. 1. A similar

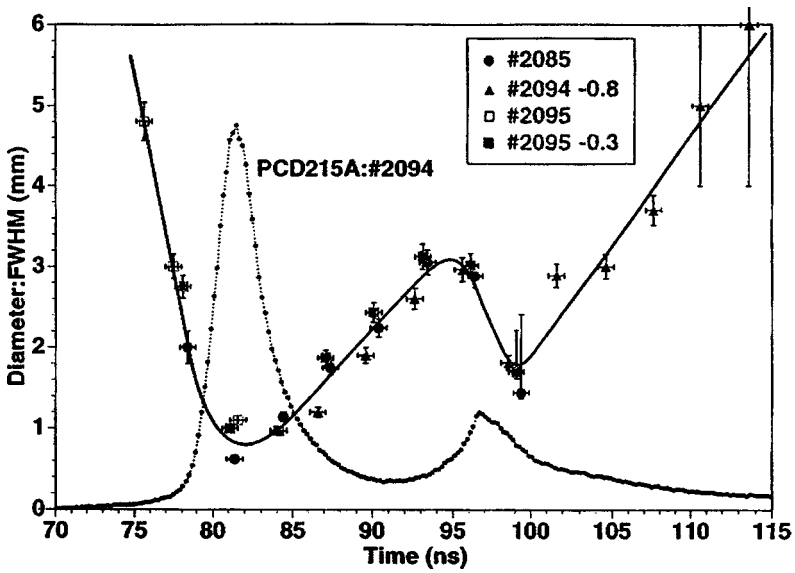

FIG. 4. The sizes of the *K*-shell emission region, inferred from pinhole picture film intensities of the different shots, as a function of time. An interpolating average curve of *K*-shell emission sizes is drawn relative to the *K*-shell power curve for shot 2094.

set of data is listed in Table I. It differs slightly from the data presented in Ref. [4] because somewhat different assumptions were made about the background level of the film response, and an attempt was made to use actual powers and radial sizes for each shot rather than average values. Because the different detectors had slightly different timings and spacings, some interpolation was required to bring the line ratios and plasma sizes of each shot to the same time. A comparison of the data in Table I with those presented in Ref. [4] provides a measure of the amount of uncertainty involved in the data analysis. It leads, in turn, to uncertainties in the values of the electron temperatures and ion densities that are inferred; however, the trends that are inferred in these quantities are the same in both analyses.

Both the static calculations employed in Ref. [4] (and in generating Table I) and the hyrodynamic calculations described in Sec. IV contain a detailed description of the atomic level structure of aluminum as well as of the transport of radiation within the pinch. The atomic model for the various ionic stages of Al covers all 14 ground states and contains a total of 122 excited states. The levels are linked via electron collisional excitation and deexcitation, radiative, three-body, and dielectronic recombination, collisional ionization, spontaneous radiative decay, and, given the radiation transport calculation, photoexcitation within spectral lines. A detailed discussion of the rate equations and the methods for calculating the various atomic rate coefficients is given in Ref. [12].

A separate radiation transport calculation for each optically thick line is carried out to provide accurate photoexcitation rates and to obtain the power emitted by the pinch in the line. The accurate calculation of this latter quantity makes it possible to meaningfully compare calculated *K*-series spectra with their experimentally measured counterparts. These transport calculations also provide a figure of merit for the pinch, if the goal of an experiment is to maximize the power or yield within a specified region of the x-ray spectrum. In the present work, 163 lines are transported and the resulting rates are coupled into the overall population and energy dynamics.

The numerical method for radiation transport employed in this work is best described as probabilistic cell-to-cell photon coupling. With a traditional single-point escape probability method, the photon escape probability is computed from each numerical cell, but no attempt is made to couple photons from region to region. By contrast, the technique used in the present calculations is equivalent to an exact solution to the full multifrequency radiation transport equation. It has been described in detail elsewhere in Refs. [13–15]. For each line, a matrix C of photon coupling constants is calculated. C_{ij} is the probability that a line photon emitted from cell i is absorbed in cell j. Efficient analytic methods are used to obtain the C's for each line. In each of Refs. [13–15], the results obtained from our method were shown to agree with previously published astrophysical solutions of radiative transfer problems over a broad range of optical depths ranging from near unity to over 10^7.

From a spectrum analysis that can be carried out using the above atomic model for aluminum, one can infer spatially averaged (both radially and axially) electron temperatures

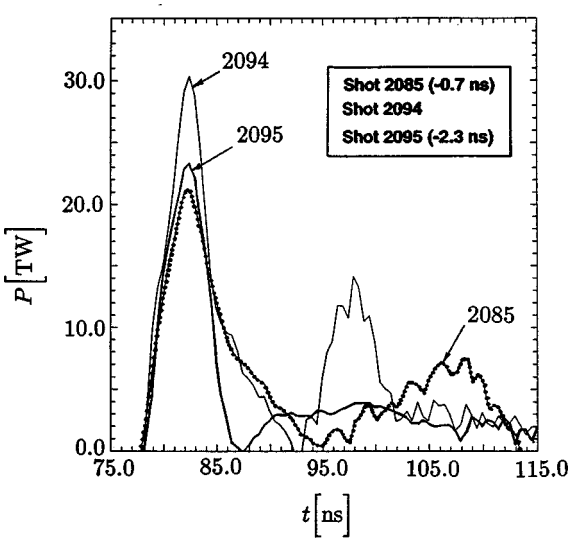

FIG. 5. Total power outputs versus time. The power pulses for the three shots are superposed by shifting shots 2094 and 2095 by the amounts indicated.

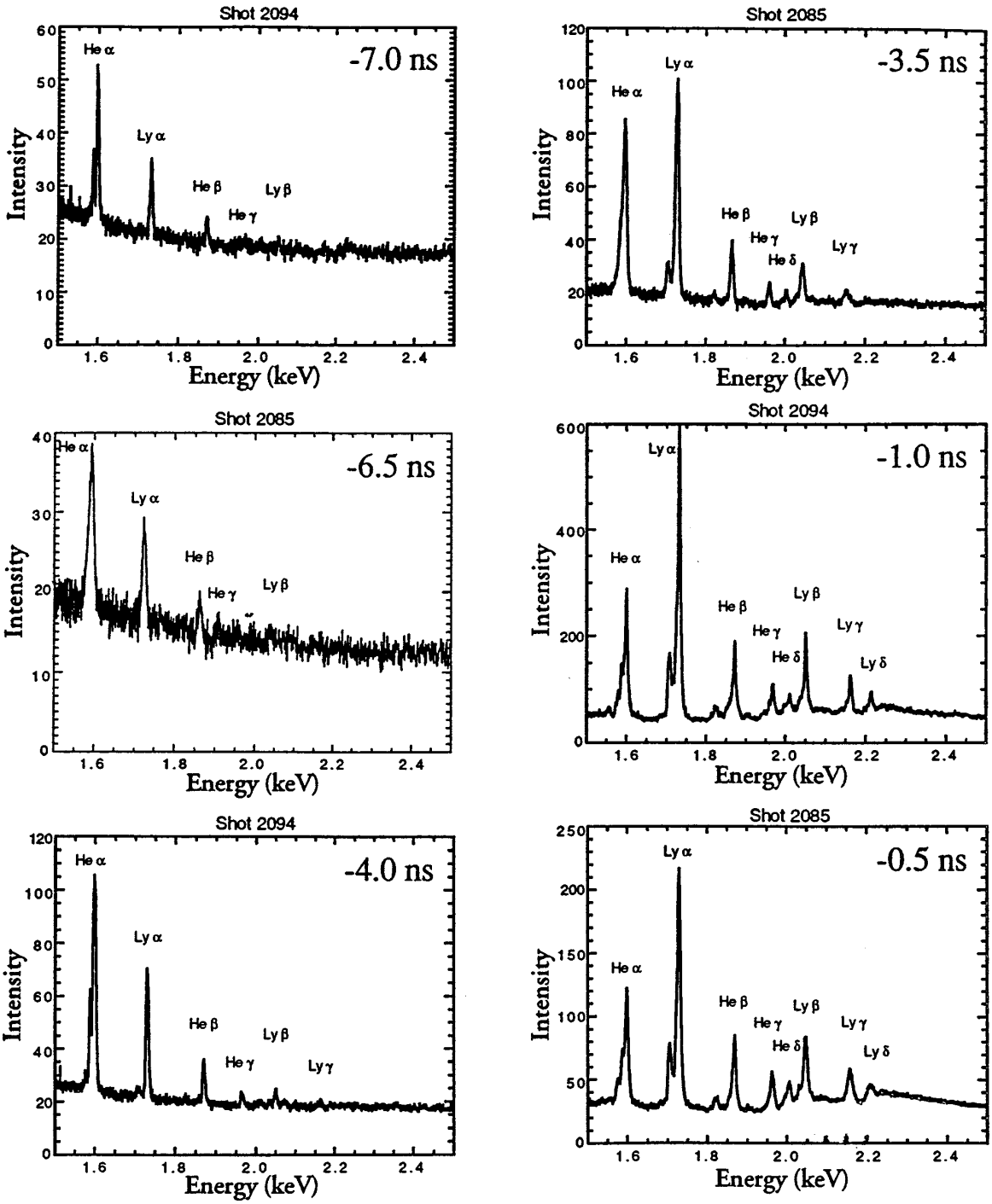

FIG. 6. Measured relative line intensities of time-resolved, aluminum, *K*-series spectra, ordered by time, for the three shots, 2085, 2094, and 2095.

and ion densities of the emission region as a function of time. These quantities are listed in Table I and discussed in Ref. [4]. The continuum analysis in Ref. [4] utilized filtered PCD data to obtain the slope of the hydrogenlike free-bound continuum as a function of time. From this slope, a second (spatially averaged) electron temperature was inferred. The combined line-continuum analyses predict comparable peak electron temperatures; however, they predict them at different times because of opacity effects. In other words, while both line and continuum x rays are generated in the hot plasma core at the time of peak compression, only the continuum can escape the plasma directly. The line emission is absorbed and re-emitted from cooler regions until the pinch expands and the plasma opacity declines. The fact that high temperatures are inferred from the line analysis at times when the plasma was expanding and the core electrons were inferred to be cooling implies a lag in ionization at these times, i.e., the ionization state is no longer in equilibrium with the cooled electrons, but reflects the earlier state of the plasma in which the electrons were hot and the plasma was in equilibrium. Electrons in the core cool too rapidly for recombination processes to maintain ionization equilibrium. However, because the line analysis implies that subkilovolt temperatures exist in the plasma at times when the plasma is

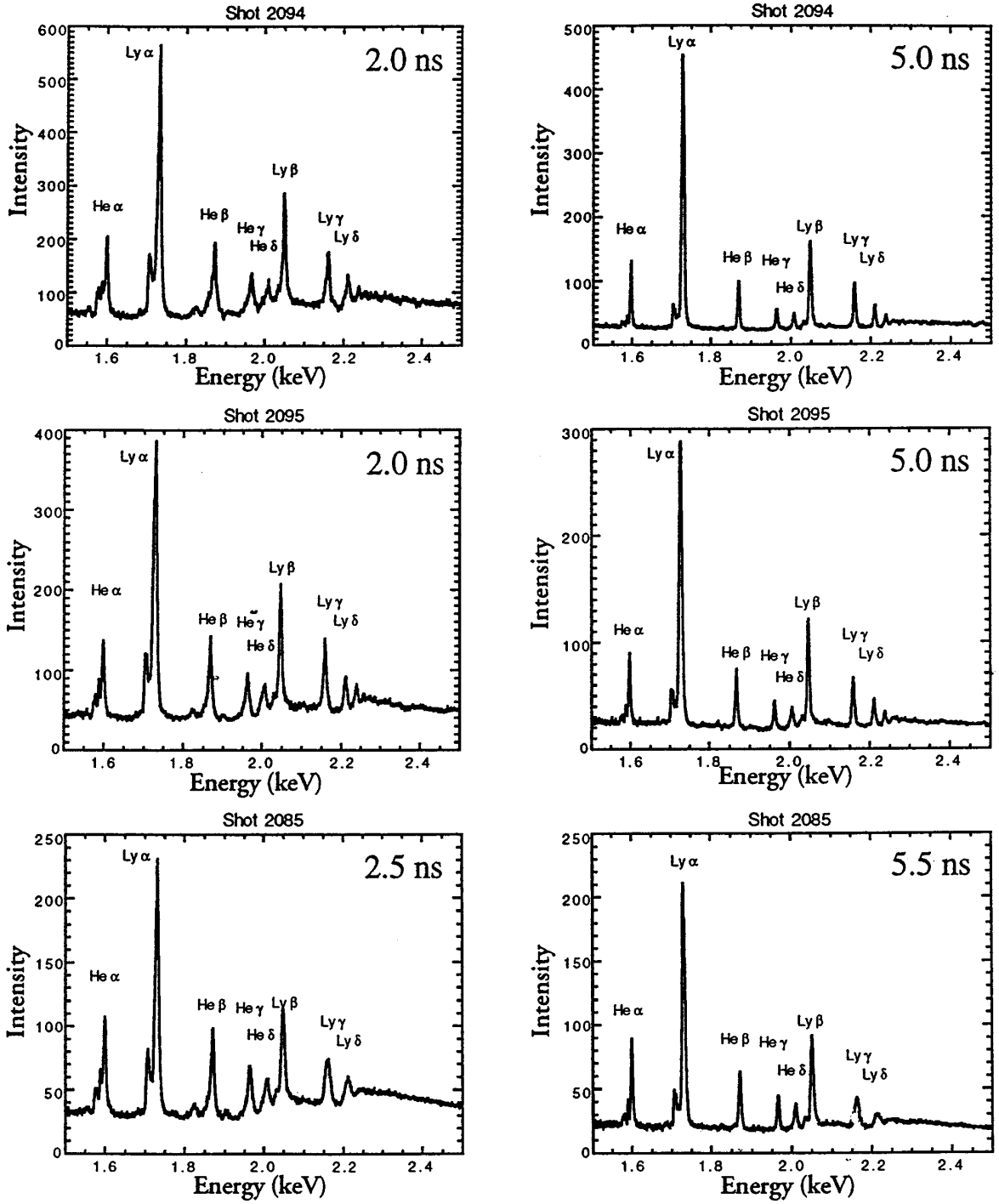

FIG. 6 (*Continued*).

approximately in equilibrium and when the continuum analysis predicts superkilovolt temperatures, the combined analysis predicts kilovolt temperature differences over submillimeter distances.

One can take the analysis of Ref. [4] a step further to strengthen this conclusion about the existence of temperature gradients. Because the size of the emission region is measured as a function of time and used in the analysis, one can use these sizes to infer emission region masses. Thus, from the average ion densities and sizes listed in Table I, one obtains the average K-shell masses in time, listed in Table I and displayed in Fig. 8. This feature added to the analysis shows that only a small fraction ($\leqslant 20\%$) of the imploded mass participates in K-shell emission. The remaining $\sim 80\%$ of the array mass is either too hot or too cold to radiate in the K shell.

Finally, a power data analysis suggests, in fact, that a large fraction of the total power was generated from plasma too cold to radiate in the K shell. Significantly, the measured ratio of total to K-shell power is approximately 6. In CRE, one can compute this power ratio, as well as the K-shell power, as functions of the electron temperature and the ion density of a given sized, uniform plasma using the atomic model described above. Contour plots of the results of these

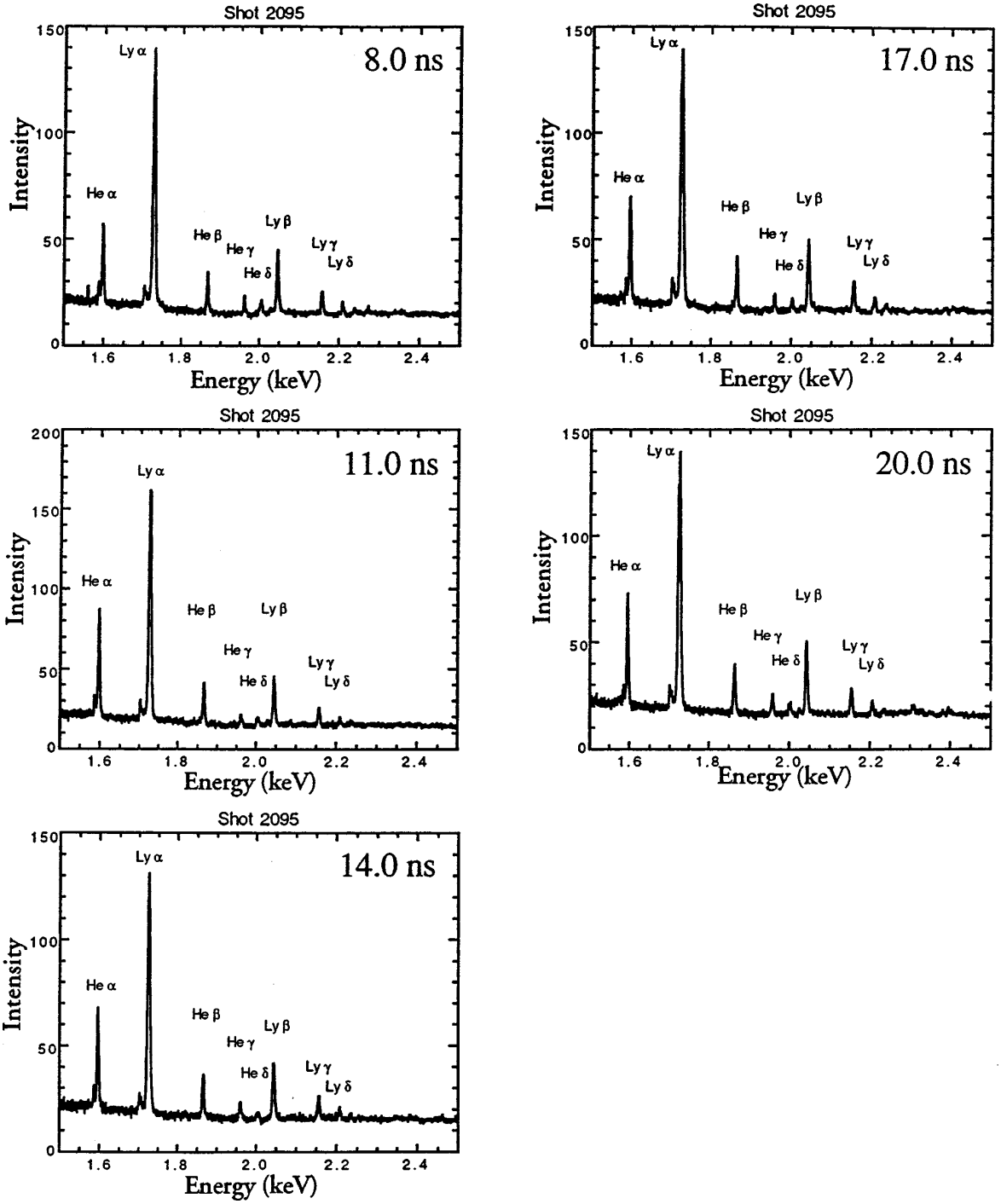

FIG. 6 (*Continued*).

calculations can then be used to determine a set of plasma conditions that are consistent with both pieces of data. The contours in Figs. 9 and 10 were obtained for a plasma 0.8 mm in diameter, which is the average diameter of the pinch at peak compression and emission from Fig. 4. Figures 9 and 10 imply that a *uniform* pinch in CRE would radiate the powers seen in Figs. 1 and 5 only if it had an average density of $\sim 1.5\times 10^{21}$ cm^{-3} and an average temperature of ~ 220 eV. In a pinch of 0.8 mm diameter, this gives a radiating mass of ~ 340 μg/cm, which is slightly larger than, but approximately equal to, the full array mass. However, these plasma conditions are inconsistent with the strength of the hydrogenlike relative to the heliumlike emissions that are also observed at peak emission (Table I). Contours for this ratio are given in Fig. 11.

Thus the power data analysis presented above (Figs. 9–11) suggests that a large fraction of the total power must be generated from parts of the plasma that are too cold to radiate significantly in the K shell. The measured ratio of total to K-shell power is too large to originate from a *uniform* plasma having the mass of the original array (308 μg/cm). Gradients in density and temperature must be present. Thus different non-RMHC analyses of the 90-wire data lead to the same conclusion, namely, that gradients are an important feature of the emission characteristics of the pinch and, therefore, of its fluid dynamics.

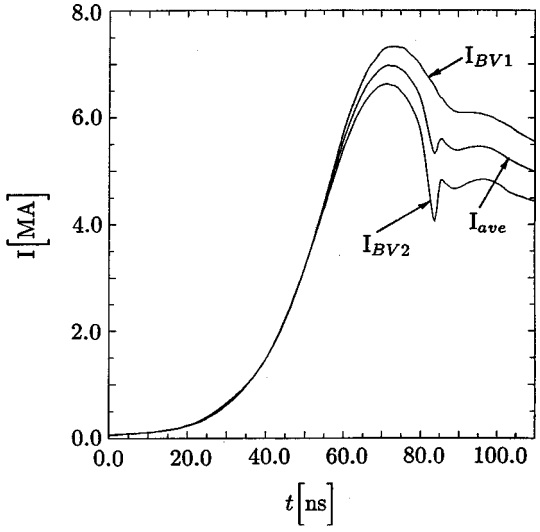

FIG. 7. Measured currents, I_{BV1} and I_{BV2}, for shot 2094 versus time. The average, I_{av}, of the two measured currents is also drawn.

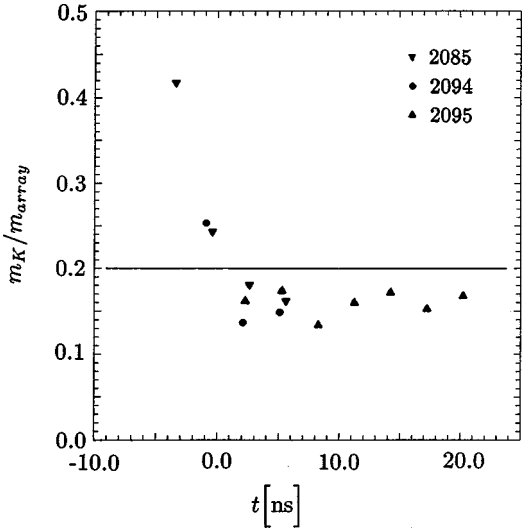

FIG. 8. Inferred fractions versus time of the mass radiating in the K shell to the total array mass.

IV. 1D RMHC DATA INTERPRETATION

Each of the data described above contains features that a reasonably accurate 1D simulation of the experiment should approximately reproduce. The K-shell and total powers, the emission region, the continuum slope temperatures, and the ion temperatures, all show evidence of a bounce and a pinch recompression that is typically seen in 1D magnetohydrodynamics (MHD) implosions. However, the strength and the time delay of the recompression are sensitive functions of the implosion dynamics as evidenced by the shot-to-shot variability of the small peak formed after the pinch bounce. 1D calculations should be able to (and do) demonstrate this sensitivity. Another important feature of the implosion, as mentioned, is the fact that the measured peak in the total power is roughly six times larger than the K-shell peak. These K-shell emissions emanate from a tight pinch. Finally, hydrogenlike dominates heliumlike emission (line and continuum) from the time of peak compression and throughout the bounce and recompression. The maximum of this relative emission is reached ~ 5 ns after the K-shell peak. 1D calculations demonstrate the sensitivity of these particular data features to different dynamical assumptions.

The analyses in Sec. III indicate the presence of radial gradients in the plasma. To determine the detailed structure of these gradients from a data analysis, one must employ RMHC calculations. While z pinches implode radially, they, in general, are three-dimensional flows that produce three-dimensional gradients. The simulation results to be presented in this section were obtained as the end result of a series of 1D RMHC implosion calculations [10] that model only the dominant, radial, fluid motion. Because they are 1D, they must assume symmetrical load accelerations, and hence they can only phenomenologically model some of the 2D or 3D effects that occur during the implosion. In addition, these calculations are driven, at least until assembly, by the Saturn electrical circuit model, which must be accurately known. The calculations are carried out from both a first principles and a phenomenological approach, i.e., 3D turbulence effects

TABLE I. Data analysis.

Shot No.	Time (ns)	Ly-α to He-α ratio	Power (TW)	Diam (mm)	$\langle T_e \rangle$ (eV)	$\langle N_i \rangle$ (10^{19} cm^{-3})	m_K/m_{array} (%)
2085	−3.5	0.58	0.71	3.6	430	2.8	42
2085	−0.5	1.21	3.7	0.8	450	33.0	24
2085	+2.5	1.98	2.5	0.7	660	32.0	18
2085	+5.5	2.75	0.98	1.6	1250	5.5	16
2094	−1.0	1.41	3.0	1.0	510	22.0	25
2094	+2.0	2.88	2.4	0.6	1220	33.0	14
2094	+5.0	5.24	0.81	1.4	1990	6.6	15
2095	+2.0	3.09	3.1	0.6	1370	39.0	16
2095	+5.0	4.16	1.1	1.4	1720	7.7	17
2095	+8.0	3.51	0.5	2.3	1700	2.2	13
2095	+11.0	2.64	0.46	2.7	1440	1.9	16
2095	+14.0	2.57	0.61	2.6	1370	2.2	17
2095	+17.0	2.24	0.78	2.3	1200	2.5	15
2095	+20.0	2.43	0.66	2.2	1245	3.0	17

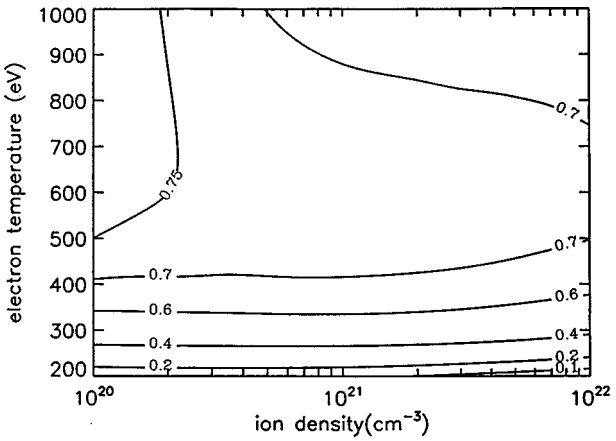

FIG. 9. Contours of the ratio of *K*-shell power to total power versus electron temperature and ion density for a uniform, 0.8-mm-diam aluminum plasma in CRE.

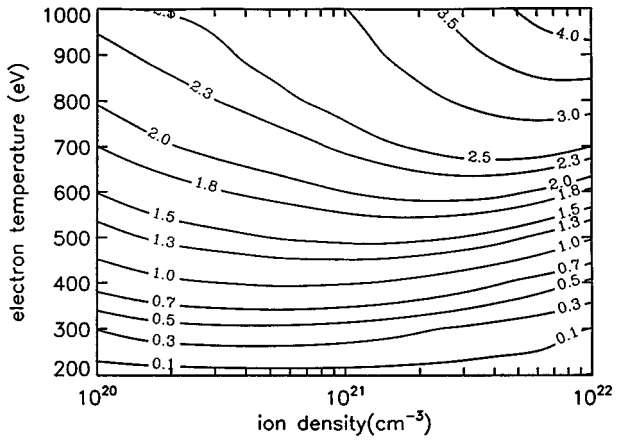

FIG. 11. Contours of the ratio of the intensities of Ly-α to the sum of He-α plus He-intercombination line emission versus electron temperature and ion density for a uniform, 0.8-mm-diam aluminum plasma in CRE.

are phenomenologically modeled by using multipliers on the classical transport coefficients (viscosity, heat conduction, and ion-electron heating term). An experimental basis for this procedure is provided in Ref. [11], where it was shown that enhancements of these quantities could be employed to bring 1D MHD calculations of *z*-pinch dynamics into better agreement with three, directly and indirectly, measured *z*-pinch quantities: (1) the average pinch density on axis, (2) the average pinch temperature on axis, and (3) the peak *K*-shell power (or measured *K*-shell yield). A theoretical basis for this procedure is that adjustments are made only to the closure terms of plasma fluid theory in order to obtain agreement with experimental data, and the closure of fluid equations is an ongoing area of research (see, for example, Ref. [16]).

The phenomenology of altering the viscosity, heat conduction, and ion-electron heating rate is employed in a 1D Lagrangian, radiation magnetohydrodynamics, computer code calculation that is described in Ref. [10]. Thirty zones were used in these calculations. The code calculates both ion and electron temperatures; it uses Spitzer conductivities and the magnetic diffusion approximation to determine the flow of current within the plasma, and it employs artificial viscosity in both the momentum and ion internal energy equations. Only artificial viscosity is employed at present, and it is implemented in accord with Schulz's tensor formulation for artificial viscosity [17]. Additionally, the calculation contains a comprehensive treatment of the ionization dynamics, described in Sec. III, together with an accurate, escape probability, description of radiation transport. These internal plasma dynamics are self-consistently coupled to each other and to the fluid dynamics [10].

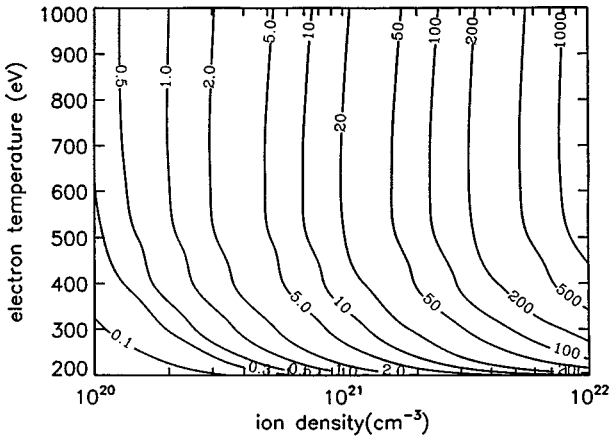

FIG. 10. Contours of the *K*-shell power output in TW/cm versus electron temperature and ion density for a uniform, 0.8-mm-diam aluminum plasma in CRE.

The goal of the 1D analysis, which is made possible by the employment of a detailed atomic model in the RMHC calculations, is to determine a set of dynamic plasma conditions that approximately reproduce the full set of time-resolved data and give, therefore, the best representation of the radial gradient structure of the plasma. The fullness of the data set is what allows, in principle, this goal to be achieved. A 1D RMHC analysis of the data proceeds by varying both the plasma initial conditions and a number of dynamical assumptions and approximations [11,18] while calculating the full set of spectroscopic data. Both kinds of variations have the effect of varying the thermalization dynamics of the plasma on axis, and these variations move the calculated data either closer to or further from the experimentally inferred data. The process can be continued until the best agreement and interpretation of the experimental data is obtained.

One approximation, that of CRE, is used in the calculations to obtain the results presented in this section, even though the above non-RMHC CRE analysis of the data strongly suggests that nonequilibrium ionization states are generated at late time in the experiment. There are two reasons for using this approximation. One, as in the initial CRE analysis of the spectral data that was given in Ref. [4] and reviewed above, these CRE-MHD calculations include the nonlocal effects of line transport, i.e., they contain photoexcitations, deexcitations, and ionizations. However, unlike the previous analysis, these photopumpings incorporate the effects of radial gradients in temperature and density. Thus only one important generalization of the previous non-RMHC analysis is made in this approximation. Two, fully

time-dependent-ionization hydrodynamics calculations are more computer intensive than CRE-MHD calculations, and thus beyond the scope of the present paper.

Since direct comparisons are made between calculated and measured spectral quantities, the 1D RMHC analysis must ultimately produce a set of plasma gradients that are consistent with, or that provide a good approximation to, the spectral data. Consistency is produced by imposing a number of physically motivated constraints on (1) the initial distribution of plasma that is generated from the exploded wire mass, (2) the calculated late-time current wave form and the resulting energy input to the pinch, (3) the strength of nonradiative, heat energy transport within the pinch and the resulting distribution of plasma energy, (4) the amount of plasma viscosity or compressibility that is generated by the plasma implosion and the resulting rate of kinetic-energy thermalization (these added amounts of viscosity are assumed physically to be generated by fluid turbulent motions), and (5) the strength of fluid-energy flow into electron thermal energy (this flow is also moderated by the presence of 3D turbulence).

Because z-pinch radiation dynamics are nonlinear, it has thus far proven difficult to obtain the goal of a very close agreement with all of the data through the adjustment of one calculational assumption at a time. However, a reasonable matchup has been achieved and is presented in this paper. The calculated powers, line ratios, free-bound continuum slopes, and the size of the plasma at peak compression are all found to be sensitive functions of the plasma initial conditions, the assumptions on the strength and distribution of plasma turbulence, and the strength of the current drive during and especially after peak compression. Each of these assumed conditions markedly affects the size of the temperature and density gradients that are generated by the calculation.

Our procedure was to begin with the pinhole data and the K-shell power data in order to determine an initial plasma distribution (that is, a given amount of precursor plasma) that would reasonably approximate the size of the plasma at peak compression as well as the width of the first K-shell pulse. We then adjusted the plasma viscosity and heat conduction to find better matches to the amplitudes of the total and the K-shell power pulses. To improve the comparisons of the ratios of these powers required some contouring of the heat conductivity and viscosity profiles. The sensitivity of 1D calculations to increases in plasma viscosity, heat conductivity, and electrical resistivity was investigated in Ref. [11]. Since each of the individual adjustments tended to affect one piece of data more than the others, their commutativity was not a major factor in our analysis. However, since changes in the assumptions regarding the plasma's initial conditions or its properties moved one or another of the calculated data toward either closer agreement or greater disagreement with the measured data, the process of seeking agreement appeared to be leading, in principle, to an unambiguous, and therefore apparently unique, set of physical assumptions offering the best matchup with the data. Ultimately, one needs to establish whether these assumptions are physically reasonable as well as unique, and that they are a generic feature of z-pinch physics that can be used in predictive as well as diagnostic, postdictive, analyses.

To begin, however, a RMHC analysis is predicated on the assumption that the energy coupling of the load to the Saturn electrical generator is known to some acceptable level of accuracy. Saturn can be characterized as a voltage generator driving a constant inductance, a line resistance, and the dynamically evolving z-pinch load inductance [19]. In a typical 1D simulation of the 90-wire experiment, the measured voltage driver and short-circuit parameters produce the load current I_L shown in Fig. 12. The average measured diode current $I_{\rm av}$ and the K-shell power pulse of shot 2094 are also drawn for comparison. Two weaknesses in this simulation are apparent from Fig. 12. One, the calculated current rise is slightly steeper than the measured rise, and two, the calculated peak is closer to I_{BV1}'s than to $I_{\rm av}$'s peak. While both measured and calculated currents dip to a minimum when the power is at its maximum at peak compression, only the calculated current exhibits a second peak. The measured current is essentially flat (and/or decaying) after pinch compression. The second peak occurs in the calculation as a result of the inductive coupling of the pinch to the generator during the pinch's reexpansion. This peak is not seen in the measured currents, even though the K-shell data indicate an expanding and then contracting emission region. One can compensate somewhat for the discrepancy between I_L and $I_{\rm av}$ by slightly reducing the driving voltage (and hence the energy input to the pinch) as was done in the calculations to be presented (shown as the dashed curve, $I_{\rm calc}$, in Fig. 12). Moreover, this voltage reduction extends the implosion time of the pinch, compensating as well for the differences in rise time between $I_{\rm av}$ and I_L.

Second, as already stated, the measured implosion time implies that the full array mass is imploded, and the strength of the total relative to the K-shell power implies only a small fraction of this mass radiates in the K shell. A significant fraction of the assembled plasma must remain relatively unheated and sufficiently cool to radiate primarily in the L shell. In this scenario, a cool plasma shell must implode onto and compress an inner region of plasma, which is then heated to superkilovolt temperatures. K-shell emissions originate from this hot region. The turn-on time of this emission is sensitive to the distribution of plasma within the inner region. Good agreement of the calculated turn-on time with the K-shell power data is achieved when the 1D calculations are initialized under an assumption that some of the wire mass is blown toward the axis by the explosion of the wires. This assumption is supported by findings in an experiment in which magnesium was coated onto aluminum wires and observed to radiate on axis a number of nanoseconds prior to the main aluminum radiation pulse and at temperatures that were higher than the aluminum [9]. Direct evidence for precursor plasma formation was also found in other experiments that were designed to investigate the early-time behavior of exploding wires [20,21]. Finally, the pinhole pictures taken in this 90-wire experiment also show the presence of precursor plasma [3].

Two examples of the end product of the 1D analysis procedure described above are provided in Fig. 13. This figure contains the temperature and density gradients that were calculated at the time of peak compression when a cool outer plasma imploded onto and heated an inner precursor plasma. These two 1D calculations, involving identical plasmas, were

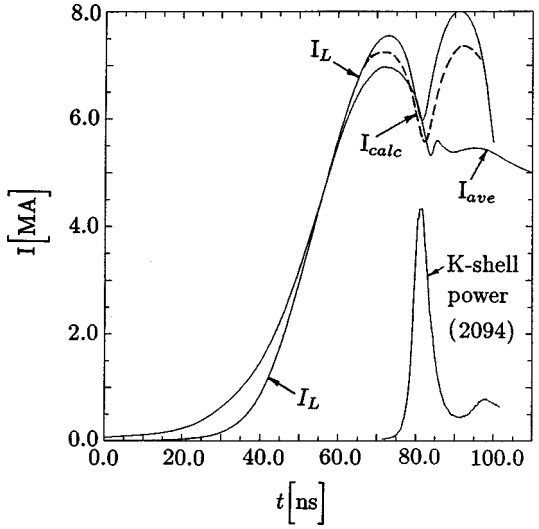

FIG. 12. The calculated load current I_L versus time in a 1D MHD calculation using the full Saturn circuit model. It is drawn relative to I_{av} and the K-shell power pulse of shot 2094 (units in Fig. 1). I_{calc} is the calculated current that is obtained by making a slight reduction in the driving voltage. It is used to drive the implosions whose results are shown in Figs. 11 and 14–17.

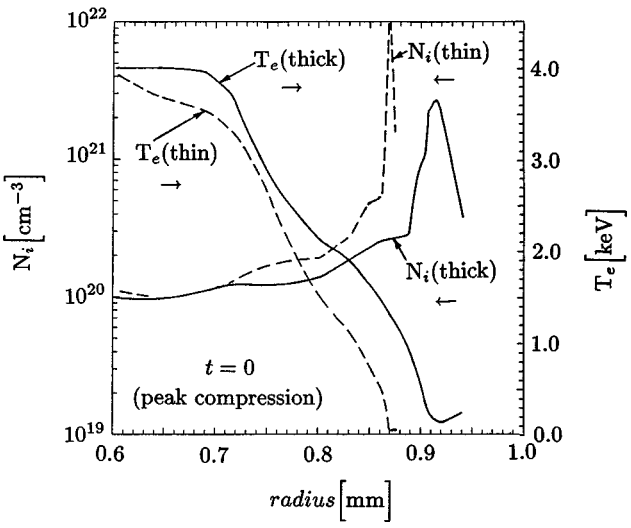

FIG. 13. Calculated temperature and ion density profiles at the time of peak compression for two calculations, identical except that in one calculation, labeled ''thin,'' all photocouplings are set to zero.

carried out under the assumptions of (1) 30 calculational zones, (2) CRE ionization, (3) a shell-like implosion with plasma inside the shell, (4) an *ad hoc* reduced energy coupling of the ions to the electrons to model the effects of 3D turbulence on energy flow to the electrons, (4) a partially enhanced, turbulence-induced, heat conduction and viscosity in the plasma interior, and (5) classical Spitzer electrical resistivity. In one of the two calculations, however, the plasma opacity was arbitrarily set to zero. This calculation shows, by contrast, how strongly plasma opacity influences the implosion dynamics and the radiation diagnostics. The initial mass distribution for the two calculations is shown in Fig. 14. 75% of the mass was concentrated around the initial position of the array, while the rest was distributed inward towards the axis. Multipliers were used to enhance the viscosity and heat conductivity of the inner zones and to reduce the flow of energy from the ions to the electrons. This reduction in electron-ion coupling modeled the effects of three-dimensional fluid and turbulence motions, since a 1D calculation is otherwise constrained to convert all of its fluid kinetic energy into ion heating. Electron-ion collisions then transfer this energy to the electrons. When there is fluid turbulence, therefore, less of the fluid energy will show up in the electrons than would otherwise be predicted in a 1D calculation.

The contouring of these multipliers that produced the best approximate agreement with the experimental data is shown in Fig. 15. The general features of the curves in Fig. 15 are more important than the detailed profiling that was used. The heat conductivity and viscosity in the outer shell of the plasma had to be assigned classical (or near-classical) values and these values had to be increased in the inner plasma region in order to achieve higher densities, lower temperatures, and subsequently, lower states of ionization in the outer shell than in the inner core region of the plasma once it assembled on axis. These assumptions and the assumed reduction in electron-ion coupling shown in Fig. 15 were necessary in order to reproduce the experimental, main, K-shell power pulse, i.e., in order to reproduce the width and amplitude of the first pulse.

The ''optically thin'' example is also given to illustrate the kind of temperature and density gradients that are more realistically needed to more closely reproduce some of the features of the spatially averaged emission data. However, this ''thin'' calculation does not reproduce the K-shell power data as Fig. 16 shows. Note that the ''optically thick'' case does reproduce the K-shell power (with a somewhat higher peak) and gives a reasonably sized (but somewhat smaller) total power pulse compared to the data. This reproduction of the K-shell pulse was obtained as a result of the assumed initial condition that a turbulent plasma had been blown in toward the axis by the early explosion of the wires. By contrast, the 2D calculations described in Ref. [3] obtain agreement with the observed K-shell pulse shape by initializing the calculation with the proper amount of random perturbation, so that a given level of 2D Rayleigh-Taylor instability is generated during the run-in. The smallness of the calculated total power in Fig. 16 may be related, in part, to the need for a more detailed atomic structure model in the L-shell. Because the 1D calculation assumes perfect implosion symmetry, however, one should expect it to produce somewhat higher radiated powers, temperatures, and densities than the experiment, which evidently has small asymmetries induced in the plasma by a measured, somewhat unsymmetric, current drive, by the finite number of return current posts, by the presence of Rayleigh-Taylor instabilities, or by wire misalignments.

When opacity is ignored, K-shell radiation losses increase by a factor of 3 (see Fig. 16). Because of this additional cooling, the plasma compresses into a tighter pinch in the ''thin'' than in the ''thick'' calculation. Thus ion densities in the outer shell are increased and electron temperatures are decreased by factors of 2 to 3. These differences in the gradient profiles significantly affect the relative amounts of hydrogenlike to heliumlike line emission that are calculated (and the average electron temperatures and ion densities that

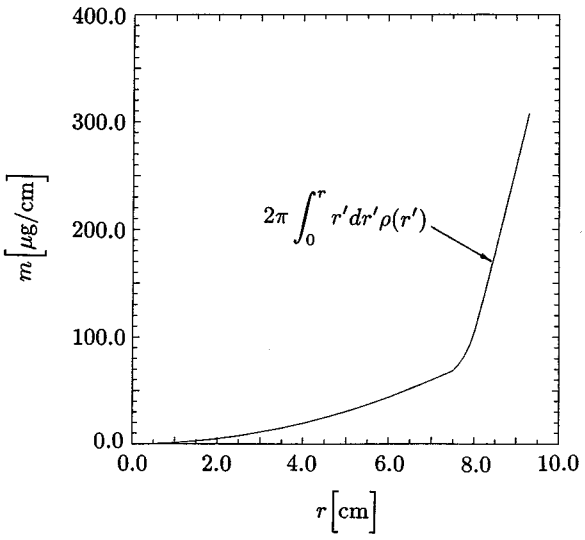

FIG. 14. The initial, integrated mass density versus radius. ~75% of the mass lies in a shell surrounding the initial array location.

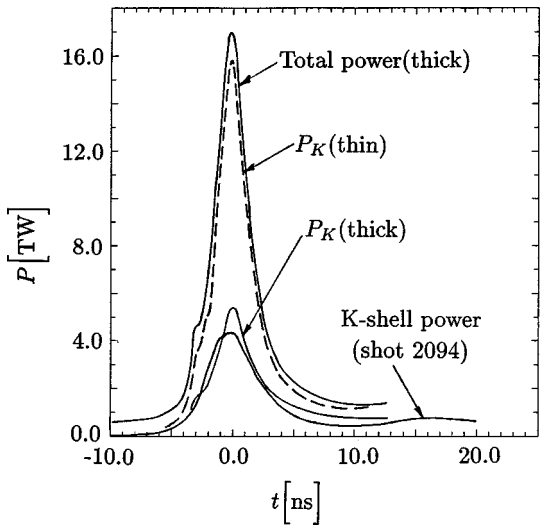

FIG. 16. The calculated *K*-shell power output for the two calculations labeled ''thick'' and ''thin'' are compared to the *K*-shell power of shot 2094. The total calculated power in the ''thick'' calculation is also shown.

would be inferred from them). These ratios are shown in Fig. 17 relative to the *K*-shell power pulse of shot 2094 and the measured line ratios that are obtained (Table I) from the time-resolved *K*-series spectra. In the CRE calculation where *K*-shell (cell-to-cell escape probability [14]) radiation transport was fully employed, the line ratios are larger than the measured values at times surrounding peak *K*-shell emission. The sharp dip in the calculated ratio, which occurs at peak compression, is an opacity effect produced by inner-shell absorption in the cooler outer shell of the plasma. By contrast, line ratios in the opacity-excluded calculation, given by the dashed curve in Fig. 17, are lower than the measured values for all times following the peak in the *K*-shell pulse.

The electron temperature $\langle T_e\rangle^{FB}$, inferred from the slope of the free-bound continuum, represents a spatially averaged

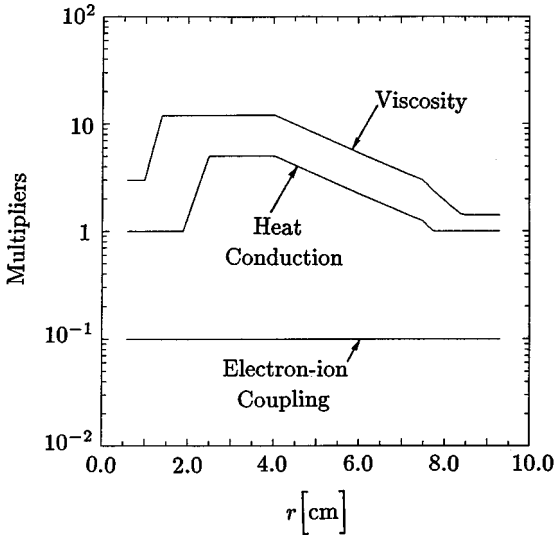

FIG. 15. The distribution of multipliers used in the calculation is shown as a function of initial position in the plasma. Both viscosity and heat conductivity are enhanced toward the plasma interior, while the electron-ion coupling rate is reduced uniformly throughout the plasma by a factor of 10.

temperature diagnostic (of the plasma core), just as the temperature inferred from a line spectrum does. Consequently, it is sensitive to the size and relative shape of temperature and density gradients as well. An average continuum temperature $\langle T_e\rangle^{FB}$ is defined by the approximation that the net free-bound emission from the plasma approximately exhibits an exponential falloff as does each individual contribution throughout the plasma. Then, the total power output per unit energy interval and per unit length, P^{FB}, is given by the following spatial integration over the plasma:

$$P^{FB}(E,t)\equiv P_0\phi(E,t)$$
$$=2\pi\int_0^R rdr\sum_{i=1}^{2} P_i^{FB}(r,t)\,\frac{1}{kT_e(r,t)}$$
$$\times\exp\{-(E-E_i)/[kT_e(r,t)]\},$$

where the profile function ϕ is defined by

$$\phi\equiv\frac{1}{k\langle T_e\rangle^{FB}}\exp[-(E-E_{\rm H})/(k\langle T_e\rangle^{FB})]$$

and satisfies

$$\int_{E_{\rm H}}^{\infty} dE\,\phi(E)=1.$$

The sum is over the two free-bound emission processes: recombination into the ground states of hydrogenlike and heliumlike aluminum. $E_{i=1}\equiv E_{\rm H}$ and $E_{i=2}\equiv E_{\rm He}$ are the locations of the free-bound edges of these processes at 2304 and 2086 eV, respectively. The power densities P_i^{FB} are obtained from the MHD calculations by the approximate expression

$$P_i^{FB}(r,t)\equiv[N_g(r,t)]_i W_i^{FB}(r,t)E_i,$$

where $(N_g)_i$ for $i=1,2$ are the ground states of totally ionized and hydrogenlike aluminum, respectively, and W_i^{FB} for

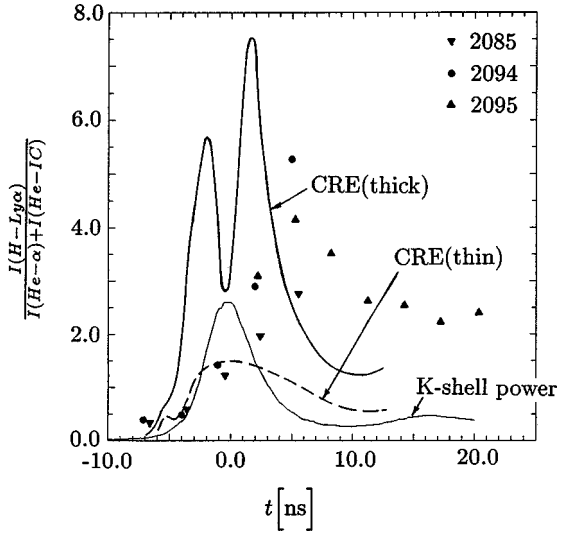

FIG. 17. The calculated ratio of hydrogenlike to heliumlike $n=2$ to $n=1$ emissions in aluminum for the two calculations labeled ''thick'' and ''thin'' are compared to the measured ratios from the three shots. The measured ratios were obtained from the spectra in Fig. 7. The K-shell power of shot 2094 is also shown for reference.

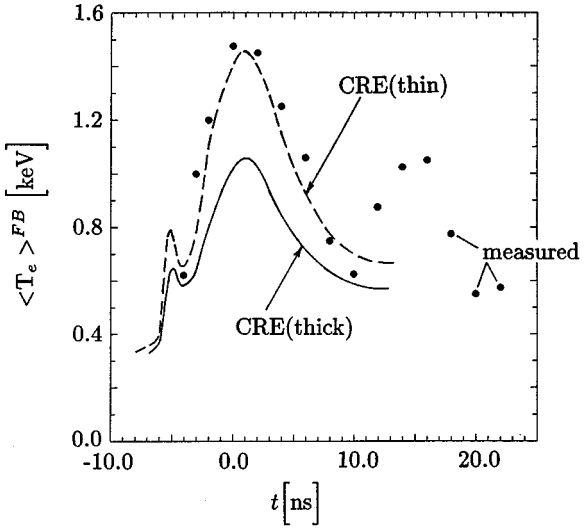

FIG. 18. Calculated continuum slope temperatures for the two calculations labeled ''thick'' and ''thin'' are compared to the temperatures (dots) that were inferred from PCD data.

$i=1,2$ are the corresponding free-bound rates for the radiative recombination processes originating from these ground states.

The above calculation for P^{FB}, carried out in the two 1D simulations discussed above, produced the temperatures shown in Fig. 18. They are drawn relative to the temperatures that were inferred from the measured slope derived from the time-resolved PCD data of Ref. [4]. Note that the average temperatures derived from the calculated ''thin'' temperature and density gradients are in agreement with the measured values. Since H-like free-bound emission is essentially optically thin in both calculations shown in Fig. 18, it depends directly on the gradients generated in a calculation and only indirectly on the plasma's opacity (through radiation reabsorption's effect on the ionization state). Thus Fig. 18 points toward a set of gradient conditions that an ''optically thick'' calculation needs to achieve in order to better match up with the observed free-bound continuum slope behavior.

Figures 15–18 suggest the insufficiency of inferring a single average electron temperature and a single ion density of an emission region that has steep gradients as was done in Ref. [4]. When large gradients are present, each piece of emission data is, in practice, indicative of only a small portion of the plasma. At temperatures of 4 keV and densities of 10^{20} ions/cm^3, the inner regions of the plasma are totally ionized and weakly emitting. At 200 eV and 10^{21} ions/cm^3, the outer plasma shell is only weakly ionized into the K shell and, again, weakly emitting above a kilovolt. Neither of these features can be diagnosed from the K-shell x-ray data. In an optically thick plasma, emission features are sensitive not only to local temperature and density, but to gradients as well.

The time-resolved spectra imply that the plasma stays hot enough throughout the time interval under study (a condition that is not observed), or that it expands quickly enough (which is observed), for the totally ionized and hydrogenlike ions to remain prevalent, since hydrogenlike line emission continues to be stronger than heliumlike. Continuum emission remains strong and concentrated in the highly ionized core of the plasma; however, its slope, which is indicative of an average electron temperature, is observed to decrease because of heat conduction, radiation losses, and expansion cooling of the core electrons. This line and continuum behavior implies (see Ref. [4]) that recombination rates were not large enough to keep the plasma core in ionization equilibrium after the pinch begins to expand and rapidly cool. This finding also appears to be supported by the 1D calculations. The calculated ratio of hydrogenlike to heliumlike emission, shown in Fig. 17, is much larger than the measured values both before and immediately after peak compression. However, this ratio falls rapidly several nanoseconds after the compression peak because the ionization balance in the calculation is forced to stay in equilibrium with the electrons as they rapidly cool. A time-dependent calculation would not be expected to show such a rapid fall, although, as mentioned earlier, such a calculation is outside of the scope of this paper.

Another way to quantify differences between calculated and measured x-ray output is to compare the amounts of line and continuum emission that contribute to the K-shell power. This breakdown is shown in Fig. 19 for the ''thick'' calculation. Note, in this calculation, that Z-to-H continuum emission (H-like free-bound) dominates over line emission, where Z represents the totally ionized aluminum ion. Measurements of this ratio would provide another important benchmark of these calculations against experiment.

Spatially resolved, but time-integrated, experimental spectra [4,8] also support the plasma picture just described. These spectra show direct evidence of a temperature gradient via the spatial dependence of H-to-He line ratios. Emissions from the axis also show a significant continuum with a slope indicative of high temperatures. This continuum is missing entirely, 3 to 4 mm from the axis (the weakness of the observed Ly-γ line at these distances also suggests low temperatures and the picture of a high-temperature core plasma

with falling temperatures away from the axis). Because of these gradients, helium-like populations are concentrated away from the axis. As the plasma is heated and ionized, ground states of heliumlike aluminum form first, then hydrogenlike ground states form in the hotter regions of the plasma nearer the axis. Because of the temperature gradient, ground states are more abundant toward the plasma surface, and opacity initially inhibits the rise in line emissions. Thus opacity displaces the way line emission reflects underlying electron temperatures, unlike the direct way the continuum slope reflects them. Pinhole pictures are similarly influenced by plasma opacity, convolving various parts of the temperature and density gradients, averaging and potentially hiding the true locations of the emission sources.

The opacity and escape probabilities of the pinch depend critically on ion temperatures. If there were no energy input to the plasma core, the ion and electron temperatures would equilibrate together typically on subnanosecond time scales; however, the ions are rapidly compressed and shock heated, and their temperatures rise faster than electron temperatures can follow. This nonequilibrium condition reduces the rate of x-ray production since energy residing in the ions cannot be radiated until it is first transferred to the electrons. This effect is pronounced in these 1D calculations because viscosity is enhanced and the ion-electron heating rate is reduced in order to model 3D fluid motions. The ion temperatures at peak compression that were computed in the ''thick'' calculation are shown in Fig. 20. The degree of nonequilibrium between electrons and ions is seen by comparing the electron temperature gradient in the ''thick'' calculation in Fig. 13 to the calculated ion gradient displayed in Fig. 20.

If, in addition to source size and instrumental broadening, one makes the assumption that the Ly-α and -β lines in Fig. 6 are Doppler and opacity broadened, a linewidth analysis [3] can be carried out that implies these lines were emitted from a region with ion temperatures on the order of 20 keV at the time of peak compression. The ''thick'' calculation's gradients in Figs. 13 and 20 support this conclusion. The source region for the Ly-α emissions, derived from the densities and temperatures of Fig. 13, is also shown in Fig. 20. The quantity $N_{2p}A_{2p\rightarrow 2s}h\nu_{2s-2p}\Delta V$ is plotted, where N_{2p} is the population density of the hydrogenlike 2p state, $A_{2p\rightarrow 2s}$ is the A coefficient for the Ly-α decay; $h\nu_{2s-2p}$ is the radiated energy, and ΔV is the volume element of the zone. In Fig. 20, the ion temperature in the zone of peak K-shell emission is 4 keV; however, the ion temperature calculated when the temperatures in Fig. 20 are averaged over the source function of Fig. 20 is 16 keV. A comparison of these source-functions-averaged ion temperatures to the experimentally inferred temperatures of Ref. [3] is given in Fig. 21. Both the experimental points and the calculated curve exhibit large ion temperatures at peak compression that decay as the plasma expands and the ions cool.

Because of the multipliers used (Fig. 15), the calculated ion temperature is not strictly a thermal temperature, i.e., it is both a measure of random microscopic motions (real ion temperature) and random macroscopic turbulence. The experimental ion temperature is similarly ambiguous because it is inferred from linewidths that may also have contributions from Doppler shifts produced either by turbulence or by radial motions. Therefore the Fig. 21 comparison between experimental and calculated ion temperatures can be viewed only as an additional assessment of how well turbulence effects are modeled in our calculations. It is an especially interesting comparison because the experimentally inferred ion temperatures were not used to constrain the 1D calculations, i.e., these temperatures did not influence our choice of transport coefficient multipliers. To compute the experimentally measured quantities directly requires a multifrequency radiation transport calculation since one must compute linewidths in a steep ion-temperature gradient in order to replicate the same information processing present in the experimental plasma spectrum. If such large (effective) ion temperatures are present at stagnation, it is important that they be diagnosed in order to promote greater understanding of the physics that takes place in the core of these plasmas. Thus experiments that can discriminate between line broadening due to thermal as opposed to fluid motions should be performed (such as counting neutrons produced from a z-pinch plasma seeded with deuterium and tritium).

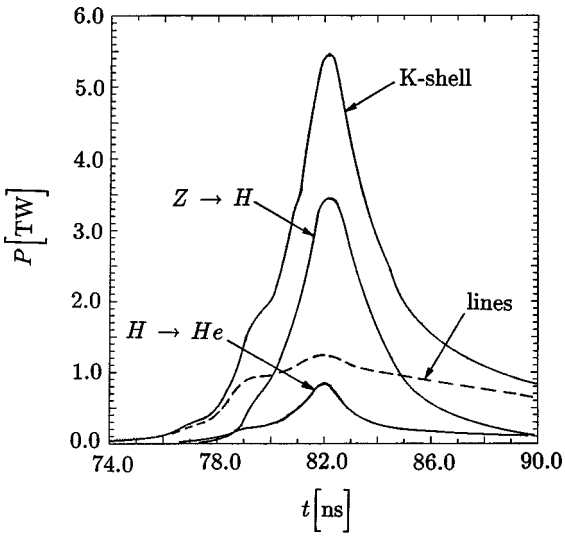

FIG. 19. The calculated K-shell power pulse from the ''thick'' calculation is broken down into its three component parts: (1) the sum of all resonance line emissions, (2) continuum emission from Z to H radiative recombination, and (3) continuum emission from H to He radiative recombination.

V. CONCLUSIONS

The picture that emerges from the 1D MHD analysis, whose general features were described and illustrated above, depends critically on various pieces of the data. To begin with, the measured and the calculated implosion times and the measured and calculated diode currents are consistent only if all the load mass implodes to the axis. However, a calculation that implodes the full load mass must also show agreement with the time-resolved K-shell pinhole pictures and the small fraction of the total mass predicted to radiate in the K shell. These pinhole pictures show that the brightest emissions come from a shell of plasma just before plasma assembly [3]. During and after peak compression, this shell of emission becomes a cylinder that pinches to a diameter of less than 1 mm and rebounds to a diameter of 3 mm before undergoing a secondary collapse to a diameter of 2 mm.

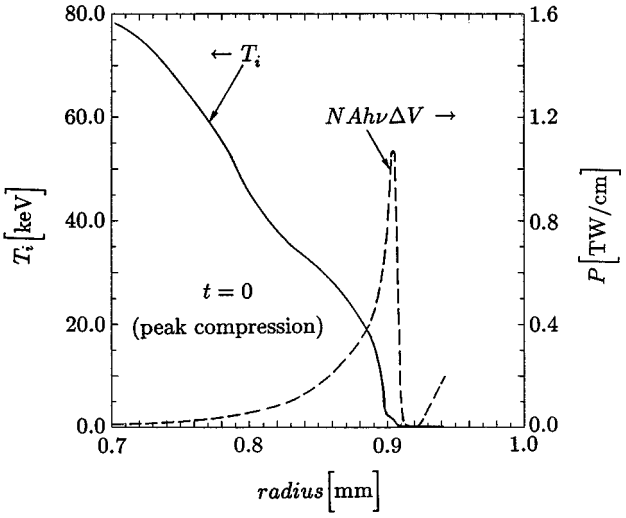

FIG. 20. Calculated ion temperature gradient at the time of peak compression. The dashed curve shows the source function profile of the Ly-α emission also at the time of peak compression.

In order to agree with the relative magnitudes of total to K-shell powers seen in the 90-wire experiment, 1D calculations have to assume that a shell of plasma implodes onto precursor plasma. In these calculations, the inner plasma with an enhanced viscosity then gets heated to much higher temperatures than the shell, whose viscosity is not enhanced. For the most part, the core is ionized in advance of the shell and becomes fully ionized. The gradient in temperature that is created persists throughout stagnation. At the time of maximum compression and emission, the peak in the number of hydrogenlike $2p$ states occurs just inside the density peak of the shell, and it falls off rapidly in the shell. Thus the plasmas in Fig. 13, like the experimental plasma in Fig. 3, produce a significant fraction of subkilovolt x rays from the cold shell surrounding the hot core.

Physically, to produce this cool shell in a 1D calculation,

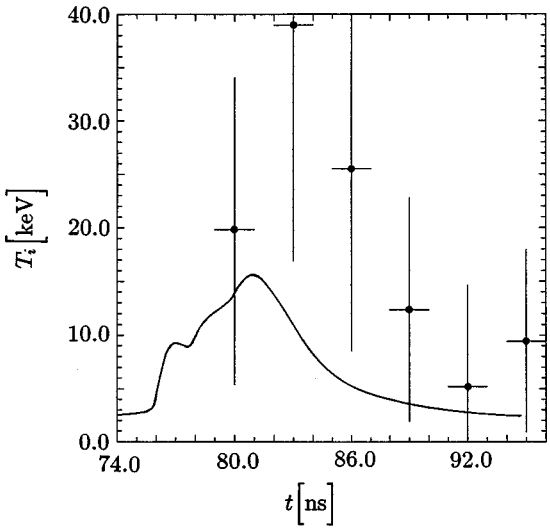

FIG. 21. Calculated average ion temperature as a function of time. The average is weighted by the source function of the Ly-α emission. The dots are the ion temperatures inferred from the measured $\Delta\lambda/\lambda$ of the Ly-α and -β lines. The measurements have large error bars as shown (see Ref. [3]).

it is necessary to assume that the shell is less turbulent than the plasma that is driven towards the axis early. Less turbulence means lower levels of viscosity and heat conduction in the shell than in the core, producing a cooler, denser plasma shell than otherwise [11]. This assumption is consistent with the 2D analysis described in Ref. [6], which shows that, early in time, the exploded wires merge into an approximate shell (in which less shearing subsequently occurs) of uniformly imploded plasma only when the spacing between wires is small enough ($\leqslant$1.4 mm). The x-y MHD calculations in Ref. [6] do show the production of a small precursor plasma, and experiments (including this one [3]) demonstrate its existence [20,9,21]. Under the assumption that it is produced during the early breakdown of the wires, one can also assume that its early inward motion produces shearing and that its collection on axis is more turbulent than that of the main body of plasma.

The optically thick CRE calculation produced approximately the right amount of K-shell emission and somewhat less total emission than shot 2085. However, the calculated pinch was approximately twice the size of the measured pinch (Fig. 13). In part, this is due to the fact that the precursor plasma in these calculations was compressionally heated to kilovolt temperatures. These temperatures impeded further compression when the denser shell imploded onto it. The agreement between the calculated and measured continuum temperatures (at peak compression) in Fig. 18 came from optically thin free-bound emission from the dashed temperature and density profiles that are shown in Fig. 13, i.e., from the profiles of a cooler, denser, smaller plasma core. Thus a better mass division between the hot core and the cold shell (with more mass in the shell and less in the core) should produce a tighter pinch and better overall agreement with the power, line ratio, and continuum slope data. The problem of finding this division will be pursued in the future. The ''optically thin'' calculation that produced the dashed set of the curves in Figs. 17 and 18 was totally artificial; the principal K-shell lines are thick under any reasonable set of assumptions regarding pinch conditions. However, as noted in the discussion of Fig. 18, the ''thin'' calculation does point the way towards further improvement in the agreement of the full, ''optically thick'' CRE calculation with the data. Another improvement is expected when this non-LTE (LTE denotes local thermodynamic equilibrium) optically thick calculation is replaced by a (non-LTE) fully time-dependent, optically thick ionization calculation.

The 90-wire experiment is a small radius experiment in which Rayleigh-Taylor instability is seen, prior to plasma assembly on axis, having a size that is compatible with the width of the first x-ray burst [3]. This observation is also compatible with the use of different levels of plasma perturbation with which to initialize 2D RMHC calculations in order to drive different levels of Rayleigh-Taylor instability to achieve agreement between the calculated and measured x-ray pulse widths of different wire-number experiments [6]. However, it has not yet been substantiated from an analysis of pinhole pictures of different wire-number experiments whether different numbers of wires (in the same array mass, same radius experiment) generate different levels of Rayleigh-Taylor growth of bubbles and spikes or whether they produce different plasma initial conditions and different

amounts of turbulent precursor plasma upon which the pinch implodes. It is by this latter mechanism that the 1D calculations of this paper reproduced the observed x-ray pulse width of the 90-wire experiment. In this 1D approach, Rayleigh-Taylor instability growth is modeled as a mechanism for generating or enhancing plasma turbulent motions that are described in a 1D calculation as modifications of the plasma's viscosity, heat conduction, and electron-ion coupling. The x-ray pulse width is then a function of the plasma's compressibility and confinement time, which, in turn, depends on the radiation loss rates of the plasma.

While only classical transport coefficients are used in 2D models (they generate their own turbulent flow), there is a question, nevertheless, as to the amount of numerical viscosity enhancement that takes place in a 2D code calculation due to the numerical diffusion inherent in a Eulerian code or due to rezoning when this numerical technique is employed. In comparing 2D RMHC calculations with z-pinch experiments, therefore, one must be mindful that numerical viscosity may also be present in calculations that use the size of an initial perturbation to control the amount of Rayleigh-Taylor induced 2D turbulence needed to reproduce x-ray pulse widths. 1D models that use classical transport coefficients and that inherently lead to radiative collapse behavior, i.e., to too high a density and radiative power at stagnation, obviously fail to get measured pulse widths right. This collapse behavior often occurs in 1D models when classical transport is used; however, reasonable agreement with a large variety of z-pinch experiments is obtained when enhanced viscosities are used in 1D modeling to phenomenologically model the presence of fluid turbulence [11]. Moreover, experience with trying to make 1D Eulerian models compare well with 1D Lagrangian models when simulating highly radiating conditions also suggests that significant enhancement of viscosity in a Lagrangian code is needed in analogy with the 2D situation. Nevertheless, no matter how turbulence effects are taken into account to simulate the x-ray pulse width in 1D or 2D RMHC calculations, one must bear in mind that pulse width is a function of interwire gap spacing as demonstrated in Ref. [6] and therefore a 3D effect. An (r,θ)-induced turbulence cannot, in principle, be explained (only modeled or simulated) by an (r,z) or (r) calculation.

To summarize, it would be highly beneficial if gradient (rather than average) conditions could be diagnosed in z-pinch plasmas. Then, it would be possible to better define or to reduce the limitations on the x-ray conversion efficiency that were seen, for example, in the 90-wire experiment (only 20% or less of the array mass participated in K-shell emission). However, in the absence of an understanding of some of the underlying influences on the plasma dynamics, a wide variety of gradients can be hypothesized. This number can be winnowed if realistic gradients could be approximately calculated using the nonlinear fluid dynamics of the pinch. The analysis of the 90-wire experiment described in this paper is based on the use of a full set of time-resolved spectroscopic data to guide in the choice of either the dynamical assumptions, the hydrodynamic zoning, or the ionization dynamic modeling that must be done in z-pinch fluid calculations in order to replicate the data. In this way, an indirect diagnosis of the underlying pinch dynamics can be carried out, and the temperature and density gradients they produce can be inferred.

The requirement that all the experimental data be replicated places significant constraints on the assumptions that can be made leading towards what appears to be a promising method for diagnosing z-pinch temperature and density gradients. Moreover, the values that were obtained for the phenomenological multipliers, which were also inferred by the 1D calculation's ability to approximately replicate *all* the data, suggest a graded turbulence structure and the influence of a precursor plasma. Clearly, more experiments and data analyses of the kind described in this paper are needed to establish the viability of this description of the implosion dynamics and to determine whether it has the ability to predict useful trends in plasma properties that can be correlated to the observed trends in x-ray emission as a function of load parameters. The ability to accurately predict some of these trends might lead to a significant improvement in our understanding of z pinches.

ACKNOWLEDGMENTS

This work was sponsored in part by the Defense Special Weapons Agency and in part by the Department of Energy.

[1] M. C. Coulter, K. G. Whitney, and J. W. Thornhill, J. Quant. Spectrosc. Radiat. Transf. **44**, 443 (1990).

[2] J. P. Apruzese, K. G. Whitney, J. Davis, and P. C. Kepple, J. Quant. Spectrosc. Radiat. Transf. **57**, 41 (1997).

[3] T. W. L. Sanford, T. J. Nash, R. C. Mock, R. B. Spielman, K. W. Struve, J. H. Hammer, J. S. De Groot, K. G. Whitney, and J. P. Apruzese, Phys. Plasmas **4**, 2188 (1997).

[4] T. W. L. Sanford, T. J. Nash, R. C. Mock, R. B. Spielman, J. F. Seamen, J. S. McGurn, T. L. Gilliland, M. Vargas, K. G. Whitney, J. W. Thornhill, P. E. Pulsifer, and J. P. Apruzese, Rev. Sci. Instrum. **68**, 852 (1997).

[5] T. W. L. Sanford, G. O. Allshouse, B. M. Marder, T. J. Nash, R. C. Mock, M. R. Douglas, R. B. Spielman, J. F. Seamen, J. S. McGurn, D. Jobe, T. L. Gilliland, M. Vargas, K. W. Struve, W. A. Stygar, J. H. Hammer, J. S. De Groot, J. L. Eddleman, K. G. Whitney, J. W. Thornhill, P. E. Pulsifer, J. P. Apruzese, D. Mosher, D. L. Peterson, and Y. Maron, in *Proceedings of the 10th International Conference on High-Power Particle Beams, Prague, Czech Republic, June 10–14, 1996*, edited by K. Jungwirth and J. Ullschmied (Academy of Sciences of the Czech Republic, Prague, 1996), pp. 146–149.

[6] T. W. L. Sanford, G. O. Allshouse, B. M. Marder, T. J. Nash, R. C. Mock, R. B. Spielman, J. F. Seamen, J. S. McGurn, D. Jobe, T. L. Gilliland, M. Vargas, K. W. Struve, W. A. Stygar, M. R. Douglas, M. K. Matzen, J. H. Hammer, J. S. De Groot, J. L. Eddleman, D. L. Peterson, D. Mosher, K. G. Whitney, J. W. Thornhill, P. E. Pulsifer, J. P. Apruzese, and Y. Maron, Phys. Rev. Lett. **77**, 5063 (1996).

[7] R. B. Spielman, Rev. Sci. Instrum. **66**, 867 (1995).

[8] T. J. Nash, C. Deeney, T. W. L. Sanford, R. B. Spielman, J. F.

Seamen, J. S. McGurn, D. Jobe, R. C. Mock, and T. L. Gilliland, J. Quant. Spectrosc. Radiat. Transf. (to be published).
[9] C. Deeney, P. D. Lepell, B. H. Failor, S. L. Wong, J. P. Apruzese, K. G. Whitney, J. W. Thornhill, J. Davis, E. Yadlowsky, R. C. Hazelton, J. J. Moschella, T. Nash, and N. Loter, Phys. Rev. E **51**, 4823 (1995).
[10] J. W. Thornhill, K. G. Whitney, and J. Davis, J. Quant. Spectrosc. Radiat. Transf. **44**, 251 (1990).
[11] J. W. Thornhill, K. G. Whitney, C. Deeney, and P. D. LePell, Phys. Plasmas **1**, 321 (1994).
[12] D. Duston and J. Davis, Phys. Rev. A **23**, 2602 (1981).
[13] J. P. Apruzese, J. Davis, D. Duston, and K. G. Whitney, J. Quant. Spectrosc. Radiat. Transf. **23**, 479 (1980).
[14] J. P. Apruzese, J. Quant. Spectrosc. Radiat. Transf. **25**, 419 (1981).
[15] J. P. Apruzese, J. Quant. Spectrosc. Radiat. Transf. **34**, 447 (1985).
[16] G. W. Hammett and F. W. Perkins, Phys. Rev. Lett. **64**, 3019 (1990).
[17] W. D. Schulz, J. Math. Phys. (N.Y.) **5**, 133 (1964).
[18] J. W. Thornhill, K. G. Whitney, J. Davis, and J. P. Apruzese, J. Appl. Phys. **80**, 710 (1996).
[19] J. Katzenstein, J. Appl. Phys. **52**, 676 (1981).
[20] I. K. Aivazov, V. D. Vikharev, G. S. Volkov, L. B. Nikandrov, V. P. Smirnov, and V. Ya. Tsarfin, Fiz. Plazmy **14**, 197 (1988) [Sov. J. Plasma Phys. **14**, 110 (1988)].
[21] E. J. Yadlowsky, J. J. Moschella, R. C. Hazelton, T. B. Settersten, G. G. Spanjers, C. Deeney, B. H. Failor, P. D. Lepell, J. Davis, J. P. Apruzese, K. G. Whitney, and J. W. Thornhill, Phys. Plasmas **3**, 1745 (1996).